



## L-SUBSHELL COSTER–KRONIG YIELDS MEASURED WITH SYNCHROTRON RADIATION

HÉCTOR J. SÁNCHEZ, ROBERTO D. PÉREZ, MARCELO RUBIO and GUSTAVO CASTELLANO

Facultad de Matemática, Astronomía y Física, Universidad Nacional de Córdoba, 5000 Córdoba, Argentina

(Accepted 15 May 1996)

**Abstract**—The synchrotron photoionization method was applied to measure  $L$ -subshell Coster–Kronig yields. This method is based on the capability of tuning the energy of the synchrotron photons producing a selective subshell ionization. Two foil samples of Yb and Ta were irradiated and their characteristic spectra were recorded. Data were analyzed using a new formalism (based on a matrix representation) for expressing X-ray fluorescence intensities involving Coster–Kronig transitions. The results obtained in this work are  $f_{12} = 0.249 \pm 0.021$ ,  $f_{13} = 0.408 \pm 0.055$  and  $f_{23} = 0.186 \pm 0.040$  for Yb, and  $f_{12} = 0.168 \pm 0.039$ ,  $f_{13} = 0.322 \pm 0.072$  and  $f_{23} = 0.161 \pm 0.053$  for Ta. These data are very reliable and represent a valuable information for spectroscopists, considering the lack of data for  $L$ -shell parameters. Copyright © 1996 Elsevier Science Ltd

### INTRODUCTION

When a vacancy in an atomic inner shell is created, the atom de-excites through a cascade process composed of radiative and non-radiative emissions. One of these processes is known as the Coster–Kronig transition, which is the fastest that exists in atoms.

Coster–Kronig decay involves electronic transitions between subshells in an atomic shell. They are labeled as  $f_{ij}^x$  denoting the probability that an electron, in the  $X_j$  subshell of the  $X$  shell, fills a vacancy in the  $X_i$  subshell. Emission processes following a Coster–Kronig transition involve mainly weakly bound electrons. In addition, a very small emission probability of low-energy photons exists.

Coster–Kronig transitions are of importance in both fundamental atomic physics and experimental applications. In particular, X-ray spectrochemical analysis needs an accurate knowledge of such transition probabilities when  $L$ -line emissions have to be measured.

Theoretical and experimental values of Coster–Kronig yields are scarce and very difficult to obtain. Usually, they present large uncertainties, and discrepancies between theoretical and experimental data are observed.

The most common methods for measuring atomic parameters of the  $L$ -shell are the coincidence techniques. These methods analyze the coincidence of  $L$ -shell emissions with  $K$ -shell photons or nuclear radiation. By means of coincidence techniques good results are obtained for some  $L$ -subshell coefficients, but this method cannot be used for determinations of

Coster–Kronig yields associated with the  $L_1$  subshell because the  $L_1 \rightarrow K$  transition is forbidden.

In recent years, Synchrotron Radiation (SR) has been used to measure  $L$ -shell Coster–Kronig transition yields (Jitschin *et al.*, 1989; Sorensen *et al.*, 1989, 1991) (simply denoted as  $f_{ij}$ ). In addition, Werner and Jitschin (Werner and Jitschin, 1988) have reported Coster–Kronig yields and ratios of fluorescence yields for  $L$ -shell in heavy atoms using the synchrotron photoionization method. This method is based on selective photoionization of subshells taking advantage of the high degree of tunability of synchrotron radiation.

As an improvement to the coincidence techniques, this method allows one to obtain all Coster–Kronig coefficients in multiple shells. Moreover, X-ray fluorescence measurements are improved by using synchrotron radiation since higher signal-to-noise ratios can be attained (Bos *et al.*, 1984; Gilfrich *et al.*, 1983; Iida *et al.*, 1985).

In this work we use the synchrotron photoionization method to obtain the  $L$ -shell Coster–Kronig yields for Yb ( $Z = 70$ ) and Ta ( $Z = 73$ ).

### METHOD

The method used in this work, first applied by Jitschin and collaborators (Jitschin *et al.*, 1985; Werner and Jitschin, 1988; Jitschin *et al.*, 1989), is based on the possibility of tuning the energy of the photons coming from a synchrotron source. This cannot be achieved using conventional sources like X-ray tubes, radioactive sources, etc. because the flux

is too low. The tunability of SR allows us to produce Coster–Kronig vacancy transfer to higher subshells in a controlled way. Monochromatic X-rays excite each absorption edge in an atomic subshell selectively. Vacancies may be filled through fluorescent decay, the intensity of such lines being related to primary vacancies as well as Coster–Kronig cascades.

Let us consider a multiple shell,  $X$ , composed by  $n$  subshells,  $E_{x_n}$  being the excitation energy of the least bound subshell  $X_n$  (a schematic representation for the  $L$ -shell is shown in Fig. 1). The first step of our experiment is to excite this subshell with photons of energy  $E_n$ , such that  $E_{x_n} < E_n < E_{x_{n-1}}$ . The fluorescence spectrum emitted by the sample is then recorded.

The next step consists of exciting the absorption edge  $E_{x_{n-1}}$  with photons of energy  $E_{n-1}$  such that  $E_{x_{n-1}} < E_{n-1} < E_{x_{n-2}}$  and recording the emitted fluorescence spectrum. The process is repeated up to the deepest level of the shell.

For the  $n$  fluorescence spectra measured during the process, theoretical intensities of each characteristic line must be calculated in order to relate experimental data with theoretical coefficients. If we consider a pure sample of thickness,  $d$ , incident photons of energy  $E$  and intensity  $I_0(E)$ , with incident and take-off angles of  $45^\circ$  (a typical configuration that reduces scattering), the XRF intensity emitted by the  $X_i$ -subshell is (Sherman, 1955; Shiraiwa and Fujino, 1966):

$$I_{X_i} = kD_{X_i}(E)M_{X_i}(E)Q_{X_i}(E)I_0(E) \quad (1)$$

with

$$Q_{X_i}(E) = \tau_{X_i}(E)\omega_{X_i}\Gamma_{X_i} \quad (2)$$

$$M_{X_i}(E) = \frac{1 - \exp(-(\mu(E) + \mu(E_{X_i}))\rho d\sqrt{2})}{\mu(E) + \mu(E_{X_i})} \quad (3)$$

$$D_{X_i}(E) = \begin{cases} 0 & E < E_{X_i} \\ 1 & E_{X_i} < E \end{cases} \quad (4)$$

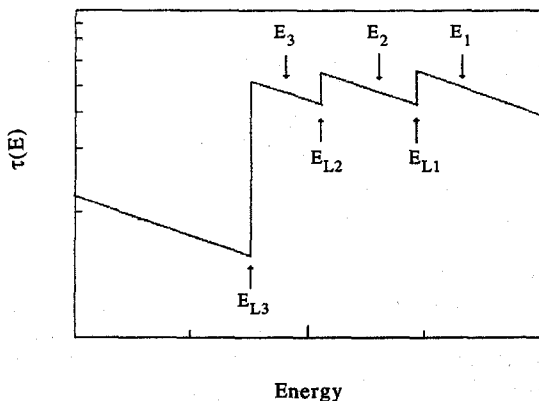


Fig. 1. Schematic representation of the synchrotron photoionization method. Photons of energy  $E_1$ ,  $E_2$ , and  $E_3$  excite selectively each absorption edge.

In the above expressions  $k$  is an experimental factor depending on the geometry and detector characteristics,  $E_{X_i}$  represents the characteristic emission energy of subshell  $X_i$ ,  $\tau_{X_i}(E)$  is the partial photoelectric absorption coefficient of subshell  $X_i$  at energy  $E$ ,  $\omega_{X_i}$  is the fluorescence yield of subshell  $X_i$ ,  $\Gamma_{X_i}$  denotes the emission probability of the characteristic line  $E_{X_i}$ ,  $\mu(E)$  represents the mass attenuation coefficient of the sample to energy  $E$ , and  $\rho$  is the sample density.

Analytical expressions for XRF intensities emitted by multiple shells contain atomic cross sections modified by Coster–Kronig effects. This is because vacancies are created not only by incident photons, but also indirectly through Coster–Kronig transitions. Coster–Kronig vacancies can be included by means of a mathematical transformation of the equations. This transformation is carried out through the following matrix system which condenses the  $n^2$  analytical expressions for the measured intensities:

$$R = AN \quad (5)$$

The matrix  $R$  represents the generated XRF intensities and the matrix  $N$  denotes the primary vacancy distribution. Matrix  $A$  takes into account the atomic emission probabilities. The elements of  $R$  and  $N$  are:

$$R_{ij} = \frac{I_{X_i}(E_j)}{M_{X_i}(E_j)} \quad (6)$$

$$N_{ij} = k\tau_{X_i}(E_j)I_0(E_j) \quad (7)$$

The matrix  $A$  can be written in terms of two matrices  $W$  and  $F$  defined by:

$$W_{ij} = \delta_{ij}\omega_{X_i}\Gamma_{X_i} \quad (8)$$

$$F_{ij} = \begin{cases} 0 & i \leq j \\ f_{ij}^* & i > j \end{cases} \quad (9)$$

where  $\delta_{ij}$  is Kronecker's Delta.

Therefore, matrix  $A$  is given by:

$$A = W \sum_{i=0}^{n-1} F^i \quad (10)$$

This expression can be understood through a careful analysis of the corresponding XRF intensities modified for Coster–Kronig transitions.

Analytical expressions for Coster–Kronig yields can be obtained using equation (5) and noting that for  $r \geq n$  is:

$$F^r = 0 \quad (11)$$

Then evaluating equation (10) we have:

$$A = W(I - F)^{-1} \quad (12)$$

As we can see, the elements of  $A$  have a simple dependence with fluorescence coefficients and Coster–Kronig yields. Hence, the knowledge of  $A^{-1}$  is equivalent to the knowledge of the atomic emission

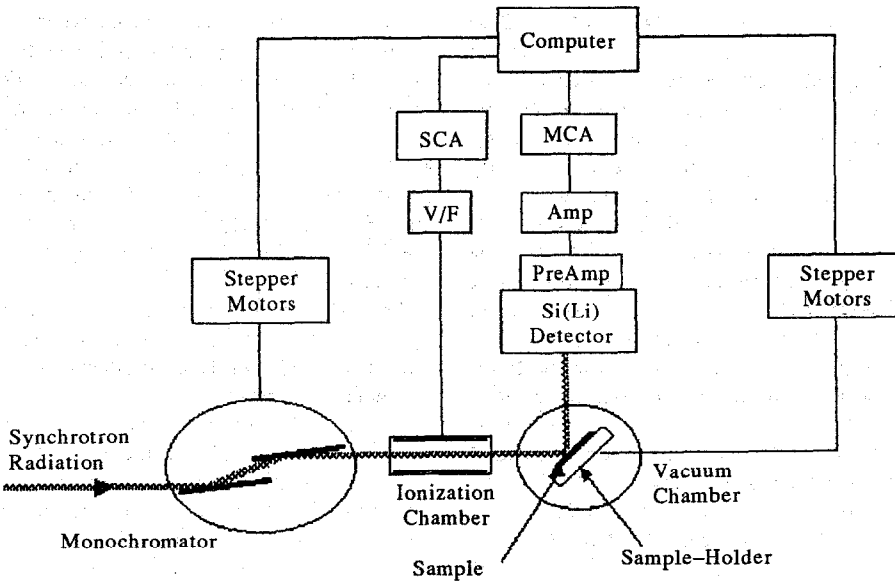


Fig. 2. Experimental setup used in this work.

probabilities. The matrix  $A^{-1}$  can be calculated by means of the following equation:

$$A^{-1} = NR^{-1}. \quad (13)$$

Note that matrix  $R$  is invertible: it is a lower triangular matrix with non-zero elements in its diagonal. Finally,  $F$  is given by:

$$F = I - A^{-1}W. \quad (14)$$

In the case of the  $L$ -shell, the above formalism reduces to:

$$R = \begin{pmatrix} \frac{I_{L1}(E_1)}{M_{L1}(E_1)} & 0 & 0 \\ \frac{I_{L2}(E_1)}{M_{L2}(E_1)} & \frac{I_{L2}(E_2)}{M_{L2}(E_2)} & 0 \\ \frac{I_{L3}(E_1)}{M_{L3}(E_1)} & \frac{I_{L3}(E_2)}{M_{L3}(E_2)} & \frac{I_{L3}(E_3)}{M_{L3}(E_3)} \end{pmatrix} \quad (15)$$

$$A = \begin{pmatrix} \omega_{L1}\Gamma_{L1} & 0 & 0 \\ \omega_{L2}\Gamma_{L2}f_{L2} & \omega_{L2}\Gamma_{L2} & 0 \\ \omega_{L3}\Gamma_{L3}(f_{L3} + f_{L2}f_{L3}) & \omega_{L3}\Gamma_{L3}f_{L3} & \omega_{L3}\Gamma_{L3} \end{pmatrix} \quad (16)$$

$$N = k \begin{pmatrix} \tau_{L1}(E_1)I_0(E_1) & 0 & 0 \\ \tau_{L2}(E_1)I_0(E_1) & \tau_{L2}(E_2)I_0(E_2) & 0 \\ \tau_{L3}(E_1)I_0(E_1) & \tau_{L3}(E_2)I_0(E_2) & \tau_{L3}(E_3)I_0(E_3) \end{pmatrix} \quad (17)$$

with

$$W = \begin{pmatrix} \omega_{L1}\Gamma_{L1} & 0 & 0 \\ 0 & \omega_{L2}\Gamma_{L2} & 0 \\ 0 & 0 & \omega_{L3}\Gamma_{L3} \end{pmatrix} \quad (18)$$

$$F = \begin{pmatrix} 0 & 0 & 0 \\ f_{L2} & 0 & 0 \\ f_{L3} & f_{L3} & 0 \end{pmatrix} \quad (19)$$

Finally,  $L$ -shell Coster-Kronig yields are written as:

$$f_{23} = \left( \frac{M_{L2}(E_2)\omega_{L2}\Gamma_{L2}I_{L3}(E_2)}{M_{L3}(E_2)\omega_{L3}\Gamma_{L3}I_{L3}(E_2)} - \frac{\tau_{L3}(E_2)}{\tau_{L2}(E_2)} \right) \quad (20)$$

$$f_{12} = \left( \frac{M_{L1}(E_1)\omega_{L1}\Gamma_{L1}I_{L2}(E_1)}{M_{L2}(E_1)\omega_{L2}\Gamma_{L2}I_{L1}(E_1)} - \frac{\tau_{L2}(E_1)}{\tau_{L1}(E_1)} \right) \quad (21)$$

$$f_{13} = \left\{ \frac{M_{L1}(E_1)\omega_{L1}\Gamma_{L1}}{I_{L1}(E_1)\omega_{L3}\Gamma_{L3}} \times \left( \frac{I_{L3}(E_1)}{M_{L3}(E_1)} - \frac{M_{L2}(E_2)I_{L2}(E_1)I_{L3}(E_2)}{M_{L3}(E_2)M_{L2}(E_1)I_{L2}(E_2)} \right) + \left( \frac{M_{L1}(E_1)\omega_{L1}\Gamma_{L1}\tau_{L3}(E_2)I_{L2}(E_1)}{M_{L2}(E_1)\omega_{L2}\Gamma_{L2}\tau_{L2}(E_2)I_{L1}(E_1)} - \frac{\tau_{L3}(E_1)}{\tau_{L1}(E_1)} \right) \right\}. \quad (22)$$

Notice that the experimental factor  $k$  was eliminated from equations (20)–(22). This implies the use of tabulated  $L$  fluorescence yields.

### EXPERIMENTAL

The measurements were carried out in the Microanalysis Station of the PWA Group of the Frascati National Laboratories (Italy). Our experimental setup is shown in Fig. 2.

The apparatus consists of an experimental vacuum chamber allowing conventional XRF (used in this work) and total reflection XRF. Inside the chamber there is a sample holder (3 × 6 cm) that can be positioned along the  $X, Y$  axis (with a precision of 5 μm) by means of two remote-controlled stepper-motors. The position is determined by two optical

encoders. At the entrance of the chamber two slits allow an orthogonal collimation of the incident beam, which comes from a six-pole wiggler and is monochromated by a two-crystal "channel-cut" monochromator. The energy resolution of the monochromator is mainly determined by the intrinsic resolution of the Si(111)-crystal (roughly 3 eV), which is extremely good for the purposes of this work. The beam intensity (about  $10^{13}$  photons/s mrad 0.1% b.w. for the critical energy) is monitored by an ionization chamber whose voltage signal is transformed to frequency pulses by a V/F converter. These values are used to correct the measured fluorescent intensities in order to avoid any instability of the electron beam. This correction is performed especially in the case of spectrochemical analyses where different measurements must be correlated. In this work it is not necessary because equations (20)–(22) do not depend on the incident intensity.

The geometry of measurements is  $90^\circ$  with  $45^\circ$  incident and take-off directions on the plane of the synchrotron electron orbit. The reason for this experimental arrangement is to minimize scattering radiation, consequently increasing peak-to-background ratios (Hanson, 1986). The detection system consists of a solid-state detector with a Si(Li) crystal (Silena), a high voltage source (Ortec 478), an amplifier (Ortec 572) and a multichannel analyzer (Ortec 916). The whole detection-system resolution is 170 eV for the  $K\alpha$  line of Mn.

The samples consist of two pure-elements foils of Yb ( $d = 0.100$  mm), and Ta ( $d = 0.100$  mm).  $L$ -fluorescent lines were measured for the samples here considered. Figures 3–5 show the measured spectra for Ta.

#### DATA ANALYSIS AND RESULTS

As mentioned in Method, the calculation of Coster–Kronig yields requires a knowledge of the intensity of three lines corresponding to decay to each  $L$  subshell. For convenience, we chose the fluorescent lines denoted as  $L\beta_{3,4}$  ( $M2, M3 \rightarrow L1$ ),  $L\beta_1$  ( $M4 \rightarrow L2$ ), and  $L\alpha_{1,2}$  ( $M4, M5 \rightarrow L3$ ) since they are the most intense lines of each group.

Experimental spectra of  $L$ -shell decay consist of three sets of fluorescent lines corresponding to vacancies in the  $L_1$ ,  $L_2$ , and  $L_3$  subshells. Each pattern of lines shares its energy interval with the other patterns. In the case of energy-dispersive spectrometers, like the one used in this work, resolution is not enough to separate all the different lines. Thus overlapping effects appear, and fitting procedures are needed to determine peak intensities. Basically, these procedures fit Gaussian functions to peaks and polynomial functions to the background. The experimental spectra were analyzed with two special programs: AXIL (Van Espen *et al.*, 1986) and SPA (Sánchez, 1991). Although these programs implemented different algorithms to achieve the fitting, the difference between the peak intensities obtained by each program was negligible. The errors of the fitted peak intensities did not exceed 1%. Calculated intensities were corrected by several factors, the most important are described below.

The first correction carried out was related to dead time. This is produced because photons arrive randomly at the detector and they have a chance to arrive during a period in which the system is not counting. We represent our detection system with a nonparalyzable model (Knoll, 1979). The calcu-

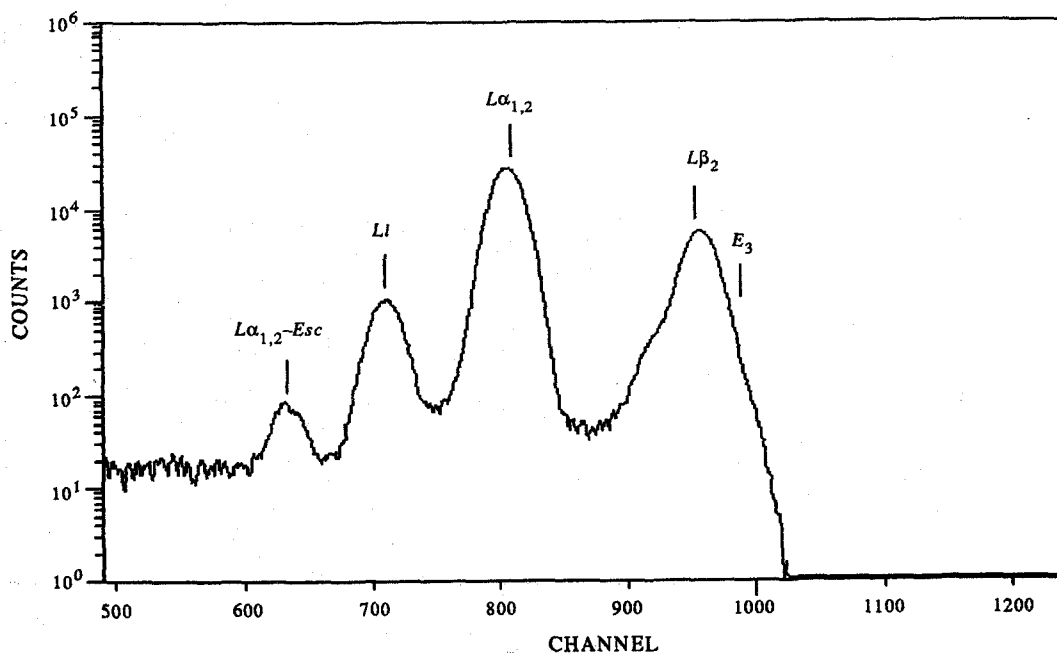


Fig. 3. The measured spectrum of Ta excited with photons of 10 keV. Only  $L_3$  lines are present.

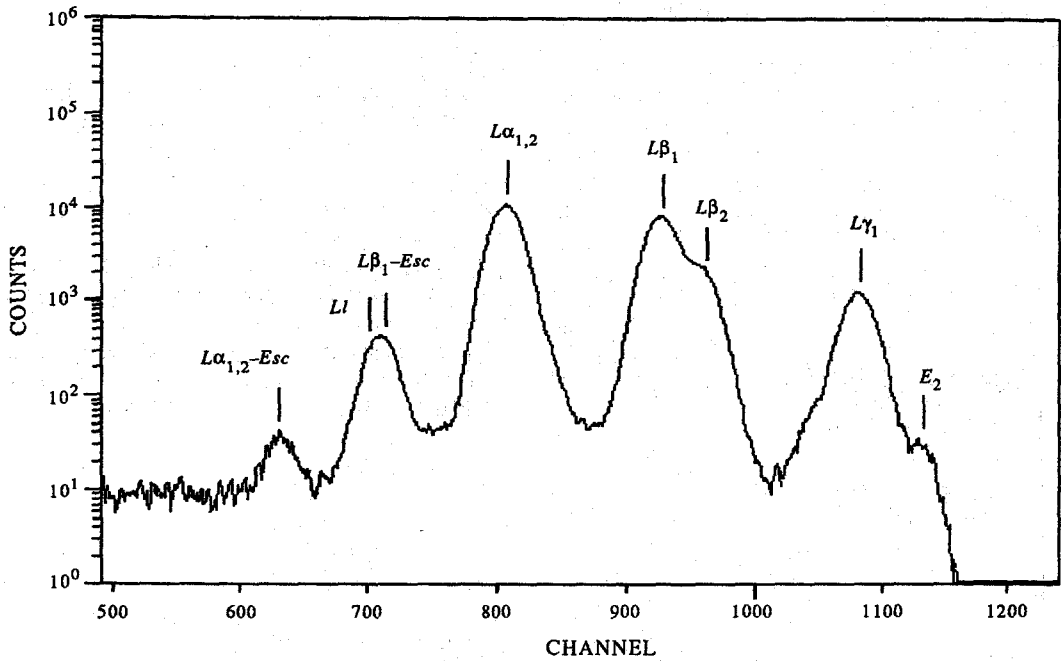


Fig. 4. The measured spectrum of Ta excited with photons of 11.4 keV. Only  $L_3$  and  $L_2$  lines are present.

lations show that this correction is negligible for the solid-state detector.

Detection efficiency was another correction considered. For the solid-state detector the detection efficiency is assumed constant in the range of energies used in this work. Therefore, the detected fluorescence intensities are proportional to the emitted ones.

Escape peaks in the fluorescence spectra were also considered. These peaks appear when the characteristic photons of Si escape from the active volume of the detector. Escape peak intensities have to be added to the calculated intensities of the principal peaks.

The last correction considered was related to secondary fluorescence. Enhancement effects were possible in all analyzed elements. It is produced

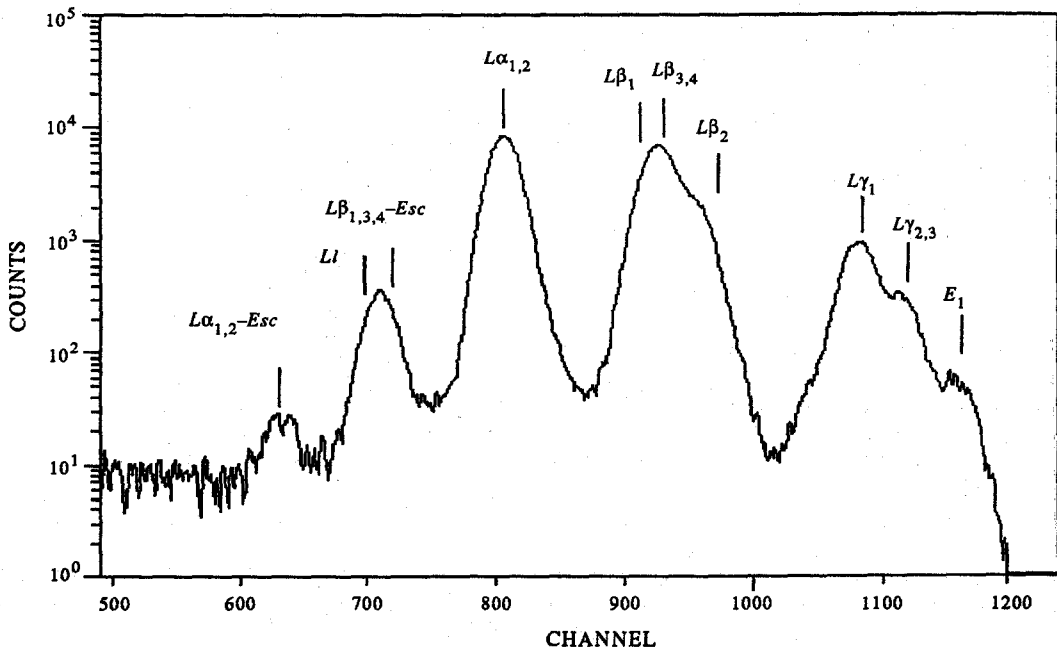


Fig. 5. The measured spectrum of Ta excited with photons of 11.8 keV.  $L_3$ ,  $L_2$ , and  $L_1$  lines are present.

Table 1. Coster-Kronig yields  $f_j$  of Yb and Ta calculated in this work, compared with theoretical and experimental data (Werner and Jitschin, 1988, Bambynek *et al.*, 1961 and Puri *et al.*, 1993)

Z		$f_{12}$	$f_{13}$	$f_{23}$
70	This work	$0.249 \pm 0.021$	$0.408 \pm 0.055$	$0.186 \pm 0.040$
	Theory	0.184	0.354	0.145
	Experimental			$0.142 \pm 0.009$
73	This work	$0.168 \pm 0.039$	$0.322 \pm 0.072$	$0.161 \pm 0.053$
	Theory	0.186	0.351	0.139
	Experimental	$0.104 \pm 0.015$	$0.339 \pm 0.020$	$0.111 \pm 0.010$

because  $L_1$  lines can excite  $L_2$  and  $L_3$  subshells, and  $L_2$  lines can excite the  $L_3$  level. Theoretical calculations of secondary fluorescence were carried out to adjust peak intensities. In most cases the correction was negligible.

Specific programs were developed to evaluate equations (20)–(22). Electron correlation effects were neglected in view of the calculations and considerations made by Werner and Jitschin in 1988.

Mass attenuation coefficients were taken from McMaster *et al.* (McMaster *et al.*, 1969; Heinrich, 1987), photoelectric cross-section for  $L$  subshells were those reported by Scofield (Scofield, 1973) and calculated as in Jitschin *et al.* (1987) and Stötzl *et al.* (1992), emission probabilities were obtained from the compilations of Scofield (Scofield, 1969, 1974) and Khan and Karimi (Khan and Karimi, 1980), fluorescence yields were taken from Bambynek *et al.* (Bambynek *et al.*, 1961) and Puri *et al.* (Puri *et al.*, 1993), and the energies of the emission lines were those compiled by Bearden (Bearden, 1969), Birks (Birks, 1974), and Bearden and Burr (Bearden and Burr, 1967).

Table 1 shows the calculated Coster-Kronig probabilities compared with experimental and theoretical values reported in the literature (Werner and Jitschin, 1988; Bambynek *et al.*, 1961; Puri *et al.*, 1993). In general they agree very well with other data from the literature. A better agreement is found for theoretical values.

Errors were estimated by propagation. Although the experimental factor  $k$  [see equation (1)] was eliminated from the equations (avoiding the poor statistics of the ionization chamber that monitored the incident beam), errors were not less than 10%.

#### FINAL COMMENTS

Synchrotron radiation has proved to be a useful tool to obtain fundamental parameters. The photoionization method is experimentally important since it is the only one that allows the simultaneous determination of all atomic decay yields associated with some arbitrary shell.

For multiple shells, fluorescence yields, emission probabilities, Coster-Kronig yields, and even photoelectric cross section usually show large uncertainties, and discrepancies exist between theoretical and experimental results. The coefficients calculated in this work are valuable information for spectro-

scopists and represent an important result considering the lack of experimental data for the  $L$ -shell parameters.

Another important result presented in this work is the mathematical formalism to express the emission equations in multiple shells. Such algebraic expressions are very simple; they are presented in matricial form and allow a better understanding of the decay formalism. Besides, this theoretical framework offers the possibility of extending the calculation technique to more complicated shells.

*Acknowledgements*—This work has been supported by the Istituto Nazionale di Fisica Nucleare (Italia) and the Universidad Nacional de Córdoba (Argentina).

#### REFERENCES

- Bambynek W., Crasemann B., Fink R. W., Freund H. U. and Mark M. (1961) *Rev. Mod. Phys.* **44**, 716.
- Bearden J. A. and Burr A. F. (1967) *Rev. Mod. Phys.* **39**, 125.
- Bearden J. A. (1969) *Rev. Mod. Phys.* **39**, 78.
- Birks L. S. (1974) *Handbook of Spectroscopy*. CRC Press, Cleveland, Ohio.
- Bos A. J. J., Vis R. D., Verheul H., Prins M., Davies S. T., Bowen D. K., Makjanić J. and Valković D. (1984) *Nucl. Instrum. Meth. B* **3**, 232.
- Gilfrich J. V., Skelton E. F., Nagel D. J., Webb A. W., Quadri S. B. and Kirkland J. P. (1983) *Adv. X Ray Anal.* **26**, 313.
- Hanson A. L. (1986) *Nucl. Instrum. Meth. A* **243**, 583.
- Heinrich K. (1987) *X-Ray Optics and Microanalysis* (Edited by J Brown and R Packwood), p. 67. Univ. of Western Ontario, Ontario.
- Iida A., Gohshi Y. and Matsushita T. (1985) *Adv. X Ray Anal.* **28**, 53.
- Jitschin W., Materlik G., Werner U. and Funke P. (1985) *J. Phys. B* **18**, 1139.
- Jitschin W., Werner U., Materlik G. and Doolen G. D. (1987) *Phys. Rev. A* **35**, 5038.
- Jitschin W., Grosse G. and Röhl P. (1989) *Phys. Rev. A* **39**, 103.
- Khan Md. R. and Karimi M. (1980) *X Ray Spectrum* **9**, 32.
- Knoll G. F. (1979) *Radiation Detection and Measurement*, p. 120. Wiley, New York.
- McMaster W. H., Kerr del Grande N., Mallet J. H. and Hubbell J. (1969) Compilation of X-ray cross sections. Report UCRL 50174, Sect. 2, Lawrence Radiation Laboratory, Livermore, Calif.
- Puri S., Metha D., Chand B., Singh N. and Trehan P. (1993) *X Ray Spectrom.* **22**, 358.
- Sánchez H. J. (1991) *Comput. Phys.* **4**, 407.
- Scofield J. H. (1969) *Phys. Rev.* **179**, 9.
- Scofield J. H. (1973) Lawrence Livermore Radiation Laboratory Report No. UCRL-51326 (unpublished).
- Scofield J. H. (1974) *Phys. Rev. A* **9**, 104.
- Sherman J. (1955) *Spectrochem. Acta* **7**, 283.
- Shiraiwa T. and Fujino N. (1966) *Jap. J. Appl. Phys.* **5**, 886.
- Sorensen S. L., Carr R., Schaphorst S. J., Whitfield S. B. and Crasemann B. (1989) *Phys. Rev. A* **39**, 6241.
- Sorensen S. L., Schaphorst S. J., Whitfield S. B. and Crasemann B. (1991) *Phys. Rev. A* **44**, 350.
- Stötzl R., Werner U., Sarkar M. and Jitschin W. (1992) *J. Phys. B* **25**, 2295.
- Van Espen P., Janssens K. and Nobels J. (1986) *Chemo. Lab.* **1**, 109.
- Werner U. and Jitschin W. (1988) *Phys. Rev. A* **38**, 4009.